HHS Public Access

Author manuscript

*Acta Biomater*. Author manuscript; available in PMC 2024 March 09.

Published in final edited form as:

*Acta Biomater*. 2024 January 01; 173: 109–122. doi:10.1016/j.actbio.2023.10.027.

# An image-driven micromechanical approach to characterize multiscale remodeling in infarcted myocardium

**Emilio A. Mendiola**[a,1], **Sunder Neelakantan**[a,1], **Qian Xiang**[b], **Shuda Xia**[c], **Jianyi Zhang**[d], **Vahid Serpooshan**[e,f,g], **Peter Vanderslice**[b,*], **Reza Avazmohammadi**[a,h,i,*]

[a]Department of Biomedical Engineering, Texas A&M University, College Station, TX, USA

[b]Department of Molecular Cardiology, Texas Heart Institute, Houston, Texas, USA

[c]Oden Institute for Computational Engineering and Sciences, Department of Biomedical Engineering, The University of Texas at Austin, Austin, TX, USA

[d]Department of Biomedical Engineering, The University of Alabama at Birmingham, Birmingham, AL, United States

[e]Wallace H. Coulter Department of Biomedical Engineering, Emory University School of Medicine and Georgia Institute of Technology, Atlanta, GA, United States

[f]Department of Pediatrics, Emory University School of Medicine, Atlanta, GA, United States

[g]Children's Healthcare of Atlanta, Atlanta, GA, United States

[h]J. Mike Walker '66 Department of Mechanical Engineering, Texas A&M University, College Station, TX, USA

[i]Department of Cardiovascular Sciences, Houston Methodist Academic Institute, Houston, TX, USA

## Abstract

Myocardial infarction (MI) is accompanied by the formation of a fibrotic scar in the left ventricle (LV) and initiates significant alterations in the architecture and constituents of the LV free wall (LVFW). Previous studies have shown that LV adaptation is highly individual, indicating that the identification of remodeling mechanisms post-MI demands a fully subject-specific approach that can integrate a host of structural alterations at the fiber-level to changes in bulk biomechanical adaptation at the tissue-level. We present an image-driven micromechanical approach to characterize remodeling, assimilating new biaxial mechanical data, histological studies, and digital image correlation data within an in-silico framework to elucidate the fiber-level remodeling mechanisms that drive tissue-level adaptation for each subject. We found that a progressively diffused collagen fiber structure combined with similarly disorganized myofiber

*Corresponding authors. pvanderslice@texasheart.org (P. Vanderslice), rezaavaz@tamu.edu (R. Avazmohammadi).

[1]These authors contributed equally to this work.

Declaration of Competing Interest

The authors declare that they have no known competing financial interests or personal relationships that could have appeared to influence the work reported in this paper.

Supplementary material

Supplementary material associated with this article can be found, in the online version, at 10.1016/j.actbio.2023.10.027

architecture in the healthy region leads to the loss of LVFW anisotropy post-MI, offering an important tissue-level hallmark for LV maladaptation. In contrast, our results suggest that reductions in collagen undulation are an adaptive mechanism competing against LVFW thinning. Additionally, we show that the inclusion of subject-specific geometry when modeling myocardial tissue is essential for accurate prediction of tissue kinematics. Our approach serves as an essential step toward identifying fiber-level remodeling indices that govern the transition of MI to systolic heart failure. These indices complement the traditional, organ-level measures of LV anatomy and function that often fall short of early prognostication of heart failure in MI. In addition, our approach offers an integrated methodology to advance the design of personalized interventions, such as hydrogel injection, to reinforce and suppress native adaptive and maladaptive mechanisms, respectively, to prevent the transition of MI to heart failure.

## Graphical Abstract

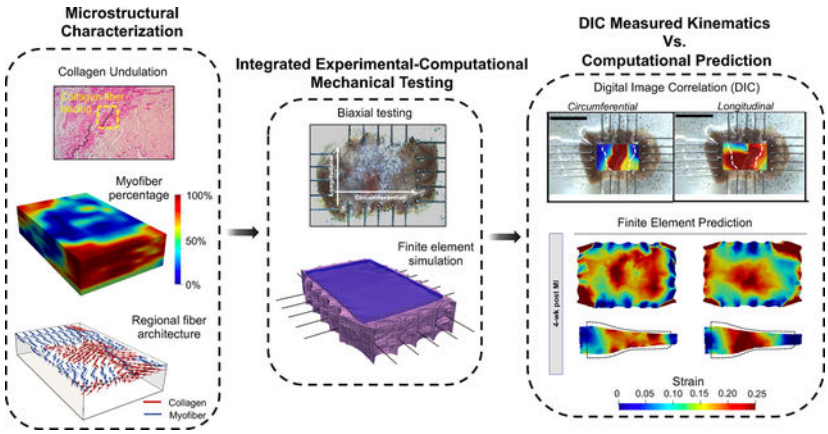


### Keywords

Myocardial infarction; In-silico modeling; Multiscale remodeling; Cardiac strains; Scar maturation

## 1. Introduction

Myocardial infarction (MI) results in cardiomyocyte death and initiates a cascade of restorative events in the myocardium, culminating in the formation of a fibrotic scar in the left ventricle free wall (LVFW). Following MI, the heart begins to heal the injured tissue of the left ventricle (LV) through the rapid addition of scar tissue, prompting changes in the content and structure of the infarcted region [1]. Additionally, the loss of contractile capacity of the LV places an increased load on the residual healthy myocardium, potentially resulting in remodeling of the remote myocardium and changes in LV chamber dimensions. Progressive remodeling of cellular and extracellular structure post-MI can lead to LV dilation, LVFW thinning, and regional fibrosis altering the biomechanical behavior of the myocardium. While scar formation may be important in reducing the risk of post-MI complications, such as excessive ventricular deformation or rupture, the normal function of the heart is strongly influenced by changes in the passive biomechanical behavior of the LVFW [2]. Excessive myocardial remodeling can have a detrimental effect on both diastolic

and systolic functions of the LV, increasing the risk of chronic heart failure (HF). Despite valuable studies on the evolution of mechanical and structural properties of MI scar tissues [3, 4], subject-specific, structure-function analysis of LVFW tissues as a whole, including infarct and remote regions and their region-specific kinematic information, remains largely unexplored.

The healing process following acute MI is a dynamic process that involves an orchestrated sequence of multiple phases, including an ischemic phase, necrotic phase, fibrotic phase, and remodeling phase [1]. Various structural alterations and remodeling events are considered to be the primary drivers of altered LVFW biomechanics in each phase. Early changes in LVFW biomechanics are dominated by the rapid increase in collagen concentration to replace necrotic tissue; however, collagen content and fiber structure may cease to be the main determinants of the biomechanical behavior of the LVFW in the late stages of post-MI remodeling [1,5,6]. Alterations in regional thickness and the formation of a sigmoidal profile, as the ventricular wall transitions from thick LVFW to a thin scar, render a key determinant of the passive behavior adaptation of the LVFW in late-stage MI. Also, structural heterogeneity and fiber alignment contribute to changes in LVFW anisotropy and directly guide LV organ-level function [7, 8]. While several studies have previously investigated the changes in LV wall passive properties and myocardium structure ([9], among others), the emphasis in previous studies has been placed on the structure and mechanical behavior of isolated scar regions. The structure-function analysis of the entire infarcted LVFW, as both mechanically and geometrically heterogeneous tissue consisting of scar, border, and remote regions, remains elusive. Such analysis proves helpful in understanding cardiac mechanics post-MI as cardiac function is driven by the behavior of the LVFW as a whole. Given the difficulty in predicting the long-term course of post-MI adaptation, the regional fiber-level analysis is critical in the differentiation between adaptive MI remodeling and that which leads to HF. Observed remodeling heterogeneity in response to MI, including sizable variability and heterogeneity between specimens [2,10,11], and uncertainty regarding the regional biomechanical alterations demand the development of a subject-specific approach that enables the integration of alterations in mechanical, structural, and anatomical features of each infarcted heart within a predictive model. The development of such individualized models serves as an essential step in improving our understanding of how regional remodeling is connected to overall myocardial behavior.

Computational modeling has shown promise in elucidating relationships between structural and anatomical remodeling events with functional outcomes. Current implementations of three-dimensional (3-D) models to simulate myocardium behavior post-MI commonly make use of phenomenological models and “lumped” representations of tissue structure. While such modeling techniques are capable of simulating an “overall” tissue-level behavior, they may fall short of differentiating between and predicting the individual contributions of myofibers and collagen fibers to tissue-level behavior [12]. The strong presence of fibrous heterogeneity, observed in scar formation [13], as well as significant regional heterogeneity of fiber content and architecture across infarcted LVFW necessitate a micromechanical approach, incorporating both regional and fiber-specific structural data, for a more rigorous and highly predictive simulation of LVFW biomechanics. Moreover, previous works studying scar formation and remodeling in the LV have indicated sizable variability between

specimens, suggesting that LVFW remodeling following MI is highly individual [14, 15], further underscoring the significance of subject-specific modeling. We hypothesize that structurally-informed subject-specific models that incorporate regional fiber data will allow for a greater understanding of the contribution of myofibers and collagen fibers to the *whole* LVFW behavior post-MI and lead to an improved understanding of the link between microstructural remodeling and LVFW kinematics.

The objective of this work is to study regional LVFW remodeling in a rodent model of MI and delineate time-evolving fiber-specific remodeling events governing tissue-level adaptations in an animal-specific manner. To meet this objective, we integrate extensive experimental data across multiple length scales through a subject-specific microstructurally informed in-silico model of the post-MI myocardium (Fig. 1). To this end, representative rat-specific finite-element (FE) models of the LVFW were developed, integrating high-fidelity regional structural data from a rodent model of MI at several progressive time-points. We compared our simulation results with ex-vivo kinematic behavior from digital image correlation (DIC) and showed that the incorporation of animal-specific architectural and geometric data is essential for the accurate prediction of myocardium biomechanical behavior. Given the often gross and limited information obtained from traditional measures of LV function and infarct dimensions, there is considerable difficulty predicting the transition from adaptive MI remodeling to chronic HF. The in-silico model presented in this work will aid in delineating subject-specific LV remodeling post-MI and assist with identifying “tissue-level” mechanistic markers that can improve the prognostic values of the traditional measures of LV performance post-MI.

## 2. Materials and methods

### 2.1. Rodent model of MI

A cohort of thirty animals was used in this study. Anteriobasal MI was induced in twenty-four 8-week-old, male, Wistar-Kyoto (WKY) rats (Charles River, Wilmington, MA) through the ligation of the left anterior descending (LAD) artery. Six animals were used as control subjects and underwent sham surgery. Animals were sacrificed at five time-points (n=6 for each group): pre-infarct (sham) and one, two, three, and four weeks post-infarct (hereafter denoted as 1-wk, 2-wk, 3-wk, and 4-wk, respectively). Subjects were anesthetized using 4% isofluorane, intubated, and connected to a ventilator. Heparin (0.2mL) was injected via the inferior vena cava and allowed to circulate for 3 minutes at which point KCl (0.2 mL) was injected to euthanize the subject. Following euthanasia, the heart was excised and perfused with a cardioplegic solution. All housing and surgical procedures were performed at the AAALAC-certified and accredited rodent care facility at the Texas Heart Institute and were performed according to protocols approved by the Texas Heart Institutes IACUC (Protocol 2021–17).

### 2.2. Mechanical characterization of the LVFW

Full-thickness LVFW myocardial specimens (in the shape of rectangular slabs) were isolated from the rat hearts (Fig. S1-I) with the slab edges being aligned with the longitudinal, circumferential, and radial directions of the LV (Fig. 2A–B). Specimens included the entire

LVFW and, as each subject had different LV dimensions, full rectangular LVFW specimens were of different dimensions (Fig. S1-II). The excised LVFW specimens were mounted in a biaxial mechanical testing machine (Cellscale Biotester) along circumferential and longitudinal directions with 1–2 mm margin behind tines (Fig. 2C–D). After mounting, the transmural thickness of the tissue specimen was measured using a micrometer while carefully avoiding compression of the tissue. The tests consisted of 10 cycles of preconditioning, followed by ten cycles of an equibiaxial loading protocol along circumferential and longitudinal directions. Forces were recorded using two 2.5 N load cells to calculate stresses. The tests were performed using displacement control, and maximum displacement was set by the stretch value (defined as the ratio of current to original dimensions along the circumferential and longitudinal directions and denoted by λ). The maximum stretch was kept at 26% to capture both linear and non-linear stress-stretch behaviors of the LVFW (Fig. 2E). The protocol was applied as a cyclic deformation with a stretch rate of 1% per second to minimize inelastic effects. The myocardial specimens were partially submerged in phosphate-buffered saline (PBS) at 20 ° C during the tests to prevent dehydration. The biaxial stresses were calculated as the first Piola-Kirchoff (1st-PK) stress. The toe region in each stress-stretch behavior was identified as the extent between no stretch to the stretch at which the stress is equal to 10% of the final maximum stress. Where appropriate the results are reported in terms of Green strain ($E$) that is related to the stretch through $\lambda = \sqrt{2E + 1}$, defined for the circumferential and longitudinal directions separately. The top surface of each tested LVFW specimen was dusted with graphite powder (Fig. 2D) to produce a speckle pattern to be used for calculating regional strains via digital image correlation (DIC).

**2.2.1. Strain calculation via digital image correlation—**Graphite dust was sprayed on the surface of the myocardium to generate a speckle pattern of various sizes and random intensity. The speckle pattern was used to track the regional variation of strain caused by the fibrotic scar and was tracked through images captured at a frequency of 1 Hz. The images were then converted to grayscale, and the change in the speckle pattern was tracked using Ncorr (open-source DIC software) to produce the displacement field. The displacement field was used to calculate circumferential and longitudinal Green strains. A representative image of the circumferential strain contour overlaid on the image is presented in Fig. 2F.

**2.2.2. Automated characterization of LVFW architecture—**After biaxial testing, LVFW specimens were fixed in 10% formalin to preserve their fibrous architecture for histological studies. The specimens were transferred to 70% ethanol after 48 hours and sectioned transmurally across the LVFW thickness (parallel to the epicardial plane). 5-μ*m*-thick slices at depth intervals of 150 um were extracted for staining (Fig. 3I–A). Slices were stained with picrosirius red (PSR), turning myofibers yellow and collagen red, and used to prepare slides (Fig. 3I–B). Slides were imaged using Olympus VS120 Virtual Slide Scanning System to obtain images at 20x to be used for architectural and area fraction quantification [16].

Two-dimensional (2-D) images acquired from stained sections were used to determine the fiber orientation distribution for myofibers and collage fibers per section using an in-

house algorithm. Previous studies have made use of similar quantification of fiber structure and indicated this histology-based method to be an accurate means to characterize fiber architecture [17,18]. A thresholding algorithm was developed to separate the yellow and red pixels (Fig. 3I–C, I–D). The yellow pixels were analyzed to compute the myofiber orientation distribution as well as the myofiber content per section (Fig. 3I–E, I–G). The yellow pixels were removed from the image, and the red pixels were used to compute the corresponding data for collagen fibers via a similar procedure (Fig. 3I–F, I–H). The helical angle $\theta$ referring to the angle from the circumferential (anterior-to-posterior) axis was chosen to identify the fiber orientation in the radial plane (parallel to the pericardial surface) with longitudinal (apex-to-base) direction representing +90° (Fig. 3I–G, I–H). 2-D fiber distributions were stacked together to generate transmural orientation probability contour plots.

PSR-stained images were used to calculate the local area fractions of myofibers and collagen fibers. Using a customized pixel-counting algorithm, we estimated both the point-wise and average area fractions of each fiber type in the specimen. The pixels that were neither yellow nor red were counted toward the ground matrix. Fields with large blood vessels were excluded from the analysis. Regional collagen and myofiber volume content were accordingly calculated as the percentage of positively stained area in the field of view.

Next, collagen fiber undulation was calculated from 2-D images. Collagen fibers in the myocardium are known to be undulated in the zero-stress state, and given their negligible bending stiffness, they do not accommodate any applied loading until recruited. The amount of collagen slack at the *fiber level* plays a key role in both the toe and high-strain regions of the stress-strain behavior at the *tissue level*. Also, collagen slack in the LVFW is expected to change by collage deposition and scar maturation post-MI whose variations remain unknown. We calculated the regional collagen fiber slack in transmural sections across the LVFW for all the time-points. Slides were imaged at 40x using a compound microscope to obtain images of the collagen fibers at different regions of each section. We defined the undulation of each collagen fiber bundle as the ratio of the distance ($D$) between two endpoints of the fiber bundle to the length of the bundle ($L$) (Fig. 3I–I, undulation = $D/L$), such that the undulation parameter lies between 0 and 1. The extreme undulation values of 0 and 1 correspond to an entirely coiled (reduced to a single point) and a perfectly straight (taut) fiber, respectively.

### 2.3. Development of subject-specific computational LVFW model

The construction of the subject-specific FE LVFW models consisted of six main steps: (i) development of a subject-specific meshed geometry with regional variation of thickness, (ii) *point-wise* subject-specific mapping of the myo- and collagen fiber content and orientations to the meshed geometry, (iii) *point-wise* subject-specific mapping of collagen fiber undulation to the meshed geometry, (iv) incorporating the fiber-specific constitutive laws that account for fiber content, orientation, and undulation, (v) replicating rake boundary conditions in silico as applied experimentally, and lastly, (vi) conducting an inverse model to estimate material parameters such that the model behavior matches experimentally measured biaxial stress-stretch response.

**2.3.1. In-silico model reconstruction and integration of structural data—**A rectangular geometry, matching the dimensions of the volume of the myocardium specimen within the rakes (approximately 10×15mm) and with a regional thickness corresponding to the measured thickness of the LVFW specimen, was meshed using linear tetrahedral elements (Fig. 3II–A). Each tetrahedral mesh contained approximately 15,000 elements. Additionally, a second set of FE models with an idealized geometry consisting of a perfect rectangular prism without varying regional thickness was developed to analyze the effect of including a true subject-specific geometry on simulated behavior. One-dimensional line elements representing the rake hooks, used in ex-vivo biaxial testing, were fixed to nodes on the perimeter of the FE model to apply displacement to the LVFW model. A fixed displacement boundary condition was prescribed to simulate the displacement applied by the hook of the rake.

High-fidelity, full three-dimensional myo- and collagen fiber content and orientation distributions, acquired from stained myocardium sections, were regionally mapped to corresponding elements in the FE model (Fig. 3II–B). Each element was assigned a primary myofiber direction (Fig. 3II–D) and a collagen fiber direction. Two factors, $\Phi_M$ and $\Phi_C$, calculated from histology and characterizing the local volume fraction of myofiber and collagen fiber, respectively, were assigned to each mesh element. Additionally, LVFW transmural collagen slack measurements, estimated from images, were assigned to the corresponding mesh elements (Fig. 3II–C). All models were assigned individual architectural and fiber content data from their corresponding representative LVFW specimens.

**2.3.2. Fiber-specific constitutive model—**A hyperelastic incompressible constitutive model of the form

$$\Psi(\mathbf{E}) = \frac{a_g}{2b_g}\left[e^{b_g(I_1-3)}-1\right] + \Phi_M\frac{a_m}{2b_m}\left[e^{b_m(I_4-1)^2}-1\right] + \Phi_C\frac{a_c}{2b_c}\left[e^{b_c\left(\frac{I_6}{\lambda_s^2}-1\right)^2}-1\right] \quad (1)$$

was used to model the LVFW passive behavior, where $a_g$, $b_g$, $a_m$, $b_m$, $a_c$, and $b_c$ are positive material constants governing the contribution of the ground matrix (g ), myofibers (m), and collagen fibers (c), respectively. $\Phi_M$ and $\Phi_C$ are weights corresponding to myoand collagen fiber volume fractions, respectively. Also, $\lambda_s$ characterizes the slack stretch of undulated collagen fibers, the point at which the fibers are fully recruited. The kinematic variables $I_1$, $I_4$, and $I_6$ are defined as $I_1 = tr\,\mathbf{C}$, $I_4 = \mathbf{f}_m \cdot (\mathbf{C}\mathbf{f}_m)$, and $I_6 = \mathbf{f}_c \cdot (\mathbf{C}\mathbf{f}_c)$, where $\mathbf{C}$ is the right Green deformation tensor, and $\mathbf{f}_m$ and $\mathbf{f}_c$ denote the local myo- and collagen fiber directions, respectively. $I_1$, $I_4$, and $I_6$ are intended to capture the deformation in the ground matrix, along myofibers, and along collagen fibers, respectively. This constitutive model, a modification of the Holzapfel-Ogden (H-O) model [19], is often used [20–23] to model the bulk hyperelastic anisotropic behavior of myocardium. The model was chosen because it incorporates terms describing the multiple fiber families for which we have architectural data. The collagen

term was modified to include a slack parameter to incorporate the behavior of undulated collagen fibers, such that the collagen fibers do not contribute to the strain energy until fully recruited at the corresponding slack stretch [24]. Additionally, the contribution of each fiber term was scaled depending on the volume fraction of the fibers at that particular element in the finite-element mesh to incorporate regional fiber-specific volume-fraction data into the model behavior. This implementation of the H-O model and our modifications allow for accurate modeling of the bulk behavior of the LVFW while incorporating the regional fiber-specific data we have collected. Given our interest in estimating myofiber and collagen contributions to myocardial mechanical behavior, we set $a_g = 0.22$ kPa and $b_g = 1.62$ as reference values for the ground matrix in LV myocardium [20] and let $\{a_m, b_m, a_c, b_c\}$ to be the material parameter variables in this work. The remaining regional material parameters, including the slack stretch, fiber factions $\Phi_M$ and $\Phi_C$, and fiber directions $\mathbf{f}_m$ and $\mathbf{f}_c$, were directly incorporated from image processing quantification (detailed in 2.2.2) into the models in a subject-specific manner.

**2.3.3. Inverse modeling to estimate material parameters—**An inverse modeling approach was used to match the experimental biaxial stress-stretch behavior. A displacement boundary condition was applied to 1-D line elements fixed to the LVFW model (simulating the rakes of the biaxial test apparatus), and FE models were stretched developing a 30% equibiaxial strain. The 1st-PK stress was calculated by summing the reaction forces at the displaced nodes and dividing them by the total area of the corresponding side at the reference configuration. The material parameters $\{a_m, b_m, a_c, b_c\}$. were estimated via a least squares optimization routine, running forward simulations to iteratively minimize the squared error between the experimentally measured stress-stretch curve and the simulated results. Models were fit to the subject-specific stress-stretch data corresponding to the particular representative LVFW specimen so that simulation predictions could be compared directly with experimental DIC data. A post-hoc parameter sensitivity test was performed in which 5% white Gaussian noise was added to the stress-stretch fitting data, and the inverse problems were run using the previously optimized material parameters as initial guesses. Values for the $b$ parameters were held constant to reduce the effect of covariance between respective $a$ and $b$ parameters intrinsic in the model [20,22,25]. The percent change between the initially optimized parameters and the parameters estimated with the fitting data, including the added noise, was calculated.

## 2.4. Statistical analysis

The experimental data were analyzed in Microsoft Excel and GraphPad Prism 9. All the data are represented as mean ± standard error of mean. The statistical significance between the circumferential and longitudinal directions in Fig. 4F was analyzed using two-way ANOVA with repeated measures and Šidák's correction. The data presented in Figs. 5A, D, and E were analyzed using one-way ANOVA with Tukey's correction when performing statistical analysis with a dependent variable. Significance was accepted at $p < 0.05$. For this study, we have chosen to report the numerical significance values [26].

# 3. Results

## 3.1. Full LVFW passive behavior adaptations

Two important changes in the biaxial behavior of the LVFW specimens that can be separately analyzed were: (i) stiffening of the tissue in the circumferential and longitudinal directions, and (ii) alterations in the toe region of the stress-stretch behavior. The sham LVFW exhibited nearly anisotropic behavior ($p = 0.0566$) with larger stiffness in the circumferential direction (Fig. 4A). LVFW anisotropy, defined as the ratio of the circumferential to longitudinal stress at the maximum stretch, was progressively reduced post-MI, with the ratio decreasing from 1.60 to 1.06 from sham to 4-wk post-MI, respectively (Fig. 4F). The toe region of the stress-stretch response (the linear response at low strains) post-MI was not significantly altered at different time-points (Table 1). The infarct region progressively tended towards a thinner profile than the remote LVFW tissue post-MI (Table 2), although only the 3-wk tissue indicated a statistically significant difference between remote and infarct thickness ($p = 0.0448$). The infarct-to-remote thickness ratio of post-MI specimens was significantly reduced when compared to the sham specimens.

## 3.2. Regional and transmural fiber specific architectural remodeling

Radially sectioned histological slices were analyzed to generate transmural volume fraction and orientation distribution for both collagen and myofibers (representative histological images from midsections are shown in Fig. 3). Scar tissue was observed in select specimens across all time-points post-MI (Fig. S3). Analysis of the fiber structure of the LVFW indicated architectural differences between time-points of the transmural variation of both collagen fiber and myofiber alignment post-MI (Figs. 5, S4). Fiber orientation quantification showed the largest change in the myofiber (Fig. S4A) and dummyTXdummy-(collagen fiber angles (measured relative to the circumferential direction, Fig. 5A) at the midwall (approximately −8° sham vs 11° 4-wk post-MI in collagen fiber angle). No significant changes were noted in the epicardium or endocardium. Myo- and collagen fibers were significantly less aligned at later post-MI time-points (Figs. 5B, S4B). The collagen fiber distribution in the full LVFW showed a similar structure as the myofibers (Fig. 5A and Fig. S4A), indicating the scar architecture conforms to the existing myofiber orientation distribution. The mean myofiber angle of the entire LVFW was not significantly altered from the sham to 4-wk time-points (approximately −7° vs 5° respectively, $p = 0.143$).

An increase in the overall collagen content of the LVFW was observed post-MI (Fig. 5D). Histological analysis indicated a transmural variation in the concentration of collagen in the sham and early MI specimens (Fig. 5C), whereas late MI time-points exhibited a nearly uniform transmural distribution (Fig. 5C). In addition to increased collagen content, the undulation distribution of the colfibers moved towards 1 (straight fibers) with the progression of time post-MI (Figs. S5, S6).

## 3.3. Region-specific LVFW deformation

Circumferential and longitudinal strain contours describing the spatial deformation of LVFW specimens during biaxial stretching showed regionally heterogeneous distribution for

all the MI specimens at medium (10%) and high (20%) strain values (Figs. 6I, S6). Remote regions of the representative post-MI specimens generally exhibited equal or reduced strain in both circumferential and longitudinal directions when compared to the sham specimens (Table S1). Circumferential and longitudinal strains in the infarct region exhibited an initial reduction compared to sham at early post-MI time-points (1-wk and 2-wk) with a subsequent increase at late MI. Scarred regions (delineated by interior region within white dashed curves in Figs. 6I, S6) tended to exhibit higher strains compared to the surrounding regions (including remote and border region tissues) after the 2-wk time-point. The contrast between the strains in scar and remote regions intensified at later post-MI time-points, indicating that the scar region is *effectively* "softer" accommodating the majority of passive strains in the stretched LVFW. In the sham specimens, the highest strain occurred at the edges of the contour due to regional thinning close to the rakes.

### 3.4. Subject-specific kinematic predictions

The inverse optimization routine estimated the passive material parameters $\{a_m, b_m, a_c, b_c\}$ (Table 3) to match the simulated circumferential and longitudinal stress-stretch relationships to the experimentally measured biaxial test results. The LVFW models were able to accurately capture the experimental stress-stretch behavior for one representative specimen per time-point (Fig. 7). The post hoc parameter sensitivity analysis indicated the maximum adjustment to a single parameter of ~9%, translating to a change in absolute value from 1.1 to 1.2 (Table S2).

The fully subject-specific LVFW computational models, informed by regional fiber content, architectural data, and varying regional thickness, were able to closely approximate the experimental strain distribution obtained from DIC (Fig. 6). The LVFW models showed regionally heterogeneous strain distribution for all the MI specimens (Fig. 6II-A-C, Fig. S7). Scarred regions in LVFW infarct models exhibited increased strains compared to the surrounding regions, including remote and border regions tissues (Tables S3, S4). At early post-MI (1-wk), the circumferential strain in the remote and infarct region was nearly the same (~4% greater in the infarct), whereas a larger alteration of longitudinal strain between regions was noted (~13% greater in the infarct). At late post-MI (4-wk), the circumferential and longitudinal infarct strain reach ~6% and ~20% greater than remote region strain, respectively.

LVFW computational models incorporating subject-specific regional thickness were able to more closely approximate the experimental strain distribution obtained from DIC in later time-points (for which infarct thinning was notable, Table 3), especially in the infarct regions (Fig. S7). In particular, the error, measuring the difference in the mean strain in the infarct region between DIC (ground truth) and FE predictions, dropped from 42%, 43%, and 27% to 26%, 10%, and 17% for 2-wk, 3-wk, and 4-wk time-points, respectively, for the circumferential strain when the subject-specific geometry was incorporated (Tables S1, S3, S4), and similar error reductions were noted for the longitudinal strains. Idealized models exhibited notably less heterogeneity and lacked the increased strain in the central scarred region that was noted in DIC. There was a reduced difference in the strain magnitude between the remote and infarct regions when comparing idealized to subject-specific

geometries (Tables S3, S4). In the 4-wk idealized models, circumferential and longitudinal strains in the infarct were ~106% and ~108% of the respective remote strains, respectively. In contrast, the subject-specific geometries exhibited infarct-to-remote strain differences of ~106% and ~120% in circumferential and longitudinal strains, respectively.

## 4. Discussion

### 4.1. Micromechanical alteration of LVFW post-MI

The myocardium possesses a complex architecture designed to produce optimal passive-active biomechanical behavior. Deterioration of LV function post-MI is driven in part by the structural remodeling and alterations of both cellular and extracellular components of the LVFW [6]. Regional increase in myocardial stiffness, brought on by increased collagen content throughout scar formation, is a well-studied phenomenon. Scar stiffness increases steadily over time, coincident with a steady increase in collagen content. In late-stage MI, however, alterations in scar stiffness no longer correlate solely with increased collagen, indicating other remodeling mechanisms take over as principal determinants of LVFW mechanical behavior [1]. Recent studies have indicated alterations in collagen undulation play a role in inducing mechanical changes in the myocardium in the setting of structural heart diseases [27,28]. Decreased collagen undulation, reducing the amount of deformation needed to activate collagen fibers, leads to a shortened toe region in the LVFW mechanical behavior, limiting the filling capacity of the LV post-MI and potentially inducing diastolic dysfunction [27]. Additionally, the structure of the newly deposited collagen fibers in the scar region and alterations of the structure of the myo- and collagen fibers in the border and remote regions (likely brought on by LV geometrical changes) contribute to changes in LVFW anisotropy. While previous studies have indicated reduced anisotropy of the scar region in rats [3], characterization of the full LVFW post-MI has not been performed. While the combination of changes in collagen structure, undulation, and content act to protect the LV from adverse events, such as LVFW rupture, extensive alterations can lead to reduced diastolic filling, impairing LV organ-level contractile function through the Frank-Starling mechanism [29].

Biaxial testing indicated the full LVFW tends toward anisotropic behavior at the sham and early post-MI time-points, with a stiffer response in the circumferential direction (Fig. 4A–B). Following MI, testing indicated a transition in LVFW mechanical behavior to an increasingly isotropic response beginning at the 2-wk time-point (Fig. 4F). Previous studies have indicated that the degree of anisotropy in LVFW scar tissue is primarily determined by the alignment of the collagen fibers [3,6]. The loss of mechanical anisotropy in the healing LVFW observed in this study was indeed supported by the diffusion of both myo- and collagen fiber orientation, as the increasingly isotropic response coincided with an increase in the spread of fiber orientation angles of the LVFW 5 B). Additionally, the bulk of the counter-clockwise shift of both myo- and collagen fiber angles was limited to the midwall region (Figs. 5A, S4A), indicating changes in tissue-level anisotropy may be highly sensitive to transmural remodeling. These coincident progressive events suggest combined alterations of myofiber and collagen fiber structure is indeed a primary determinant in the loss of anisotropy in the full LVFW. Overall, when comparing sham with 4-wk post-MI

hearts, while the mean fiber orientation of the 4-wk post-MI still tended towards the circumferential direction, the loss of fiber alignment post-MI (increased fiber spread), likely due to heterogeneous deposition of collagen fibers and geometrical remodeling, resulted in reduced tissue anisotropy. Interestingly, the reduced slack length measured via imaging in the post-MI myocardium (Table 3) compared to the sham tissue specimen is not clearly evident in the toe region of the biaxial stress-stretch relationship (Table 1). This observation, in connection with the varying collagen volume content in those time-points, suggests that, although collagen fibers are fully recruited earlier at all post-MI time-points, collagen in the infarct has been degraded and may behave effectively softer [30]. This result encourages future studies to investigate the heterogeneity of collagen degradation in the infarcted LVFW, as it is not clear if collagen degradation is isolated to the infarct region or exists in the entire LVFW, including remote tissue. Additionally, newly deposited collagen may be intrinsically softer, possibly as it is newly deposited and not yet matured. Finally, results suggest excessive LVFW thinning could act as a competing mechanism to decreased collagen undulation, potentially counteracting changes in the toe region (discussed in detail in Section 4.2). Thus, the time-course alterations in LVFW behavior are driven by a complex confluence of factors suggesting interactions between collagen content, collagen maturation and degradation, and collagen undulation play an important role in determining LVFW anisotropy in late-stage MI.

The orientation of the collagen fibers closely followed the transmural structure of the myofibers. Previous studies regarding the collagen structure of the scar region post-MI have indicated similar patterns of collagen deposition [31–33]. As the collagen fiber structure has been shown to be a major determinant of LVFW anisotropy and, consequently, diastolic and systolic LV function, recent studies have investigated the effect of particular collagen structures on the improvement of ventricular output [7]. Modeling conducted by Fomovsky et al. [7] suggested that an infarct stiff in the longitudinal direction but compliant in the circumferential direction would produce the best pump function. The modeling platform we have presented here provides an ideal structurally-informed means by which to further investigate the effect of “optimal” post-MI LVFW architectures on tissue-level function in a subject-specific manner.

### 4.2. Strain as a non-invasive metric to indicate changes in structure-function relationship

In the normal heart, myocardium regional architecture and composition in the LVFW produce an optimal passive extension in diastole, resulting in an effective contractile pattern and efficient ejection fraction at the organ level [12,34]. Remodeling of the fiber organization and collagen fiber content post-MI in the LVFW can independently alter passive kinematics of the LVFW and modulate global metrics such as cardiac output through various mechanisms, including the Frank-Starling law [29]. The altered regional deformations in DIC results support the link between fiber-level remodeling and tissue-level kinematic behavior of the LVFW at late-stage post-MI, coincident with decreased tissue thickness, and fiber reorientation and diffusion.

Interestingly, DIC and modeling predictions revealed reversed trends in the development of passive regional LVFW strains post-MI (Tables S3, S4). The scar region experienced

the maximum strain in the LVFW tissue in late-stage MI (3-wk and 4-wk time-points) whereas the remote region experienced maximum strain at early post-MI (1-wk time-point). Although the de-slacking of collagen fibers noted at late post-MI time-points is expected to curtail the excessive deformation of the scar region, the thinning of myocardial specimen in the scar region, as a maladaptive and competing mechanism to de-slacking, facilitates excessive deformation in the scar region which may lead to further thinning [35,36]. Our results indicated a reduced infarct-to-remote thickness ratio at post-MI time-points, likely contributing to the increased strain noted in the infarct region. The higher strains associated with the scar, which are likely associated with the thinning of the LVFW, are commonly accompanied by regional LV dilation which can aggravate adverse remodeling of the LV [37]. The remote LVFW tissue tended to exhibit reduced strains at later post-MI time-points. Reduced strains in the remote region can be considered to be a trade-off to increased infarct strain. As the infarct region can sustain larger strains, less deformation is experienced by the remote tissue. This may be a direct means by which increased infarct compliance leads to heart failure, as remote and border tissues are less stretched in diastole and less capable of making use of the Frank-Starling mechanisms to generate appropriate tension in the active state. Regional remodeling that influences cardiac strains, such as wall thinning, collagen content, undulation, and fiber structure, are not easily characterized in vivo. As a function of various remodeling events, LVFW strains can act as a *composite* metric to track the spatial heterogeneity of LV deformation and could be a useful tool to *non-invasively* quantify the state of remodeling in the LV [38,39]. Further detailed study of the links between individual remodeling mechanisms and LVFW kinematics is warranted as the results from this study indicate that in vivo strain tracking of the myocardium could be a valuable prognostic tool to risk-stratify MI patients.

### 4.3. Importance of subject-specific micromechanical modeling and assessment in MI

Previous works studying scar formation and remodeling in the LV have indicated sizable variability between specimens, suggesting that LVFW remodeling following MI is highly individual [14,15,40]. The contributing factors to this variability include, but are not limited to, cardiac anatomy, LVFW fibrous architecture prior to MI, the location and size of the infarct, and the heterogeneity of the infarct region. Additionally, it is unknown whether the LVFW remodeling plateaus post-MI. Indeed, the healing scarred region is an active and dynamic tissue that may never reach a stable, mature configuration that could be taken to mark the end of remodeling [1,41]. These details warrant the implementation of the subject-specific approach we have presented in this study that enables the analysis of the relationships between fiber-specific remodeling events and tissue-level biomechanical changes. This approach will serve as an essential step to develop individualized predictive models that incorporate individual data to optimize prognosis and personalize existing cardiac interventions to treat MI.

The development of models capable of accurate prediction of LVFW kinematics requires the incorporation of fiber-level structural data and subject-specific geometrical measurements. Studies have indicated accurately accounting for regional fiber heterogeneity in the post-MI myocardium is essential to accurately capture LVFW mechanics [13]. Our modeling results further indicated correct accounting for the geometry of the LVFW is key for an

accurate prediction of post-MI strains. Our results showed incorporation of regional fiber architecture, fiber volume content, and collagen undulation alterations is not sufficient to accurately estimate the increased positive strains in the infarct regions that are verified by DIC. Such a response was evident in the FE models which made use of a generic rectangular geometry without the implementation of subject-specific changes in regional thickness (Fig. S7). As DIC indicated increased scar compliance throughout the healing process, the absence of a subject-specific geometry resulted in the reduced ability of idealized models to accurately estimate the regional strain distribution revealed by DIC. The incorporation of the subject-specific thickness in the FE models resulted in a more accurate estimation of LVFW strains. The fully subject-specific models more closely matched the regional trend seen in the DIC results, indicating peak strain occurs within the thinned scar region. These results suggest there is a point in the remodeling process at which LVFW thinning overtakes the stiffening effect of increased collagen content and reduced undulation in the scar region. Together with the observations described in the previous studies [10,13], our results reinforce the importance of subject-specific assessment of remodeling and the capability of future models to identify structural metrics that aid in patient stratification in a subject-specific manner.

Thoughtful parameterization of subject-specific models holds promise to extract information regarding the contribution of *individual* remodeling mechanisms towards the complex alterations of tissue-scale behavior. The incorporation of essential parameters relating to remodeling processes provides the opportunity for analysis of time-course development of mechanisms such as changes in collagen undulation, myo- and collagen fiber volume fraction, and the mechanical contribution of each fiber family. For instance, while the representative sham and 4-wk specimens exhibited similar overall mechanical behavior at the tissue level, our combined experimental-modeling platform indicated different material parameters corresponding to distinct kinematic behavior noted at those time-points through DIC (Table 3). Similar collagen fiber volume content suggests the distinct strain responses are likely the results of a combination of changes in myo- and collagen fiber stiffness, fiber slack stretch, and geometric effects of LVFW thinning (Table 3). The lower stiffness parameters ($a$'s and $b$'s) governing the contribution of both myo- and collagen fibers in the 4-wk specimen would suggest a lower fiber strength in both fiber families and, consequently, a decreased final stress state compared to sham. However, in light of the similar stress-stretch behavior, the increased overall stress in the 4-wk specimen can be attributed to reductions in slack stretch. On the contrary, LVFW thinning in the infarct region in the 4-wk specimen (Table 3), led to a slightly extended toe region (compared to sham) (Fig. 7). These results suggest thinning acts as a competing mechanism to changes in fiber strength and undulation. Our observations reinforce the need for complete subject-specific development of myocardial models for accurate analysis of post-MI remodeling. Finally, the incorporation of parameters related to important remodeling events at the fiber level in models, such as those presented here, allows for future parametric studies useful for characterizing the current state of LVFW remodeling *in vivo* and for prediction of imminent alterations in LVFW behavior from kinematic and microstructural data acquired via imaging.

### 4.4. Translational values of the presented approach

Invasive and minimally invasive cardiac interventions for MI patients have been extensively pursued to alleviate remodeling effects post-MI. These interventions include injectable hydrogels [42–45], tissue fillers [46], and the placement of chronic pacing or constraint devices in the LV [47,48]. A key goal of such mechanical therapeutics is to curtail excessive alterations in LV passive properties and improve the properties of scarred regions to be similar to that of remote tissue. Given the evident need for patient-specific design and prognosis of these therapeutics, a quantifiable link between LVFW fiber- and tissue-level remodeling and clinically observable markers becomes increasingly desirable. However, the adaptive and maladaptive nature of fiber remodeling events and their quantifiable link to alterations to the tissue-level biomechanical behavior remains elusive. Among several translational potentials, our approach offers a platform to design personalized hydrogel injection strategies post-MI to reinforce and suppress native adaptive and maladaptive mechanisms identified in this study, respectively, to prevent the transition of MI to systolic heart failure. In addition, the structurally informed, subject-specific, modeling platform presented here serves as an essential step toward the personalized design of engineered cardiac sleeves and patches that provide optimal reinforcement of adaptive remodeling mechanisms in the host heart given the time-point-specific biomechanical status of the heart. An obstacle with such an approach is perhaps acquiring subject-specific microstructural data in vivo. Recent advances in diffusion-weighted imaging (DWI) have made the possibility of accurate in vivo characterization of myocardial microstructure a near reality [49]. Additionally, methods to predict myocardium fiber structure from cardiac strains acquired via traditional magnetic resonance imaging have been proposed that could reduce the need for complex DWI imaging sequences [50]. Although further improvement is needed, the ability to acquire myocardial microstructural data in vivo is on the horizon and will convert subject-specific modeling platforms such as those presented in this work into powerful tools for personalized therapeutic design.

Furthermore, traditional, organ-level measures of LV function, such as ejection fraction and cardiac output, have continuously fallen short of stratifying MI patients at higher risks of systolic heart failure in a timely manner. This shortcoming is primarily due to their insufficient sensitivity of organ-level to tissue-level adaptations, including fibrotic and architectural remodeling events, till such events have already extensively progressed. The tissue- and fiber-level indices introduced in this work, such as LVFW anisotropy and collagen fiber undulation, complement the traditional, organ-level measures of LV anatomy and function and hold promise to improve early prognostication of heart failure in MI. Along these lines, cardiac motion, quantified through magnetic resonance imaging or echocardiography, holds the promise to provide quantifiable assessments of tissue- and fiber-level remodeling events in the LVFW in vivo. Accordingly, previous studies have found both longitudinal and circumferential strains post-MI to be independent prognostic indicators of adverse cardiac events post-MI [38,51,52]. Future studies will include using cardiac motion indices to infer such remodeling events for subject-specific prognostication and optimal design of cardiac interventions in MI.

### 4.5. Limitations

Firstly, our approach to fiber architecture characterization through histology neglects the potential transverse component of the fiber angle. While myocardial fibers are known to maintain some degree of transverse direction, the biaxial LVFW behavior we explore in this work is dominated by the fibers laying in the circumferential-longitudinal plane. Additionally, we made use of a limited cohort of young male rats in this study (n = 6 at each time-point). Previous studies have indicated young and aged mice exhibit distinct remodeling responses to MI [53]. While a larger cohort of both male and female rats is necessary to more accurately characterize the time-course alterations of the LVFW post-MI, a power study indicated our sample size had sufficient power for accurate statistical analysis and we expect the presented significant differences to be accurate. Finally, the tines of the biaxial testing machine were not perfectly aligned for each biaxial test, possibly introducing adverse shear deformations and stresses that are not accounted for in the FE model. We do not expect the mean biaxial results to be significantly altered as a result of the misalignment of a few specimens. While the strain prediction resulting from the representative FE simulations may be slightly adversely affected by misalignment of the tines, we believe it unlikely the minor shear deformations created by the misalignment create a significant change in the qualitative differences between simulated time-points presented here. Finally, the inverse parameter optimization could be improved by the addition of an objective function making use of experimentally-derived strain data as an error metric for the estimation of material parameters. Such an error metric would be more likely to be used in future in vivo applications.

## 5. Conclusions

In this work, we took an essential step towards modeling the multiscale and subject-specific remodeling of the LVFW following MI to address the challenges of inherent spatial nonuniformity of post-MI remodeling and significant variability from subject to subject. This approach will be critical to separate the changes in the biomechanics of the LVFW caused by alterations in regional thickness from those that are due to alterations in fiber architecture, content, and undulation. This modeling approach can delineate the contributing factors of collagen deposition, collagen fiber reorientation, and thinning of LVFW in drastic alterations of LVFW mechanical behavior and anisotropy. Important connections between changes in the biomechanical characteristics and kinematic behavior of the myocardium and fiber-level remodeling events were demonstrated. Our future work will include using the subject-specific and time-point-specific modeling platform presented in this work to determine when and how adaptive remodeling transitions to heart maladaptation and, subsequently, heart failure post-MI.

## Supplementary Material

Refer to Web version on PubMed Central for supplementary material.

## Acknowledgements

This work was supported by the National Institutes of Health (K99HL138288 and R00HL138288 to R.A.). The authors acknowledge the assistance of the Integrated Microscopy and Imaging Laboratory at the Texas A&M College of Medicine.

## Data availability

The data that support the findings of this study are available from the corresponding author, R.A., upon request.

## References

[1]. Holmes J, Borg T, Covell J, Structure and mechanics of healing myocardial infarcts, Annu. Rev. Biomed. Eng. 7 (1) (2005) 223–253, doi: 10.1146/annurev.bioeng.7.060804.100453. [PubMed: 16004571]

[2]. Richardson WJ, Clarke SA, Quinn TA, Holmes JW, Physiological implications of myocardial scar structure, Comprehens. Physiol. 5 (4) (2018) 1877–1909, doi: 10.1002/cphy.c140067.

[3]. Gupta K, Ratcliffe M, Fallert M, Edmunds L, Bogen D, Changes in passive mechanical stiffness of myocardial tissue with aneurysm formation, Circulation 89 (5) (1994) 2315–2326, doi: 10.1161/01.CIR.89.5.2315. [PubMed: 8181158]

[4]. Fomovsky G, Holmes J, Evolution of scar structure, mechanics, and ventricular function after myocardial infarction in the rat, Am. J. Physiol. Heart Circ. Physiol. 298 (1) (2010) H221–8, doi: 10.1152/ajpheart.00495.2009. [PubMed: 19897714]

[5]. Holmes J, Covell J, Collagen fiber orientation in myocardial scar tissue, Cardiovasc. Pathobiol. 1 (1996) 15–22.

[6]. Fomovsky G, Thomopoulos S, Holmes J, Contribution of extracellular matrix to the mechanical properties of the heart, J. Mol. Cell. Cardiol. 48 (3) (2010) 4 90–4 96.

[7]. Fomovsky G, Macadangdang J, Ailawadi G, Holmes J, Model-based design of mechanical therapies for myocardial infarction, J. Cardiovasc. Trans. Res. 4 (2011) 82–91.

[8]. Clarke S, Richardson W, Holmes J, Modifying the mechanics of healing infarcts: is better the enemy of good? J. Mol. Cellul. Cardiol. 93 (2016) 115–124, doi: 10.1016/j.yjmcc.2015.11.028.

[9]. Li W, Biomechanics of infarcted left ventricle-a review of experiments, J. Mech. Behav. Biomed. Mater. 103 (2020) 103591. [PubMed: 32090920]

[10]. Gaasch W, Zile M, Left ventricular structural remodeling in health and disease: with special emphasis on volume, mass, and geometry, J. Am. College Cardiol. 58 (17) (2011) 1733–1740, doi: 10.1016/j.jacc.2011.07.022.

[11]. Mendiola E, Neelakantan S, Xiang Q, Merchant S, Li K, Hsu E, Dixon R, Vanderslice P, Avazmohammadi R, Contractile adaptation of the left ventricle post-myocardial infarction: predictions by rodent-specific computational modeling, Ann. Biomed. Eng. 16 (2) (2022) 721–729.

[12]. Avazmohammadi R, Soares J, Li D, Raut S, Gorman R, Sacks M, A contemporary look at biomechanical models of myocardium, Annu. Rev. Biomed. Eng. 21 (2019) 417–442. [PubMed: 31167105]

[13]. Korenczuk C, Barocas V, Richardson W, Effects of collagen heterogeneity on myocardial infarct mechanics in a multiscale fiber network model, J. Biomech. Eng. 141 (2019), doi: 10.1115/1.4043865.

[14]. Avazmohammadi R, Li D, Leahy T, Shih E, Soares J, Gorman J, Gorman R, Sacks M, An integrated inverse model-experimental approach to determine soft tissue three-dimensional constitutive parameters: application to post-infarcted myocardium, Biomech. Model. Mechanobiol. (2018), doi: 10.1007/s10237-017-0943-1.

[15]. Li D, Avazmohammadi R, Merchant S, Kawamura T, Hsu E, Gorman J, Gorman R, Sacks M, Insights into the passive mechanical behavior of left ventricular myocardium using a robust

constitutive model based on full 3d kinematics, J. Mech. Behav. Biomed. Mater. (2019) 103508, doi: 10.1016/j.jmbbm.2019.103508. [PubMed: 32090941]

[16]. Neelakantan S, Xiang Q, Li CS,K, Ling X, Dixon R, Sacks M, Vanderslices P, Avazmohammadi R, Abstract 14303: structural remodeling in the left ventricular myocardium underlies systolic dysfunction in myocardial infarction, Circulation 144 (Suppl_1) (2021), doi: 10.1161/circ.144.suppl_1.14303. A14303–A14303

[17]. Hsu EW, Muzikant AL, Matulevicius SA, Penland RC, Henriquez CS, Magnetic resonance myocardial fiber-orientation mapping with direct histological correlation, Am. J. Physiol.-Heart Circulat. Physiol. 274 (5) (1998) H1627–H1634, doi: 10.1152/ajpheart.1998.274.5.H1627.

[18]. Liang X, Elsaid N, Jiang L, Roys S, Puche A, Gullapalli R, Stone M, Prince J, Zhuo J, Direct cardiac compression devices to augment heart biomechanics and function, Speech Lang Hear Res. 17 (2022) 3661–3673, doi: 10.1044/2022_JSLHR-22–00040.

[19]. Holzapfel GA, Gasser TC, Ogden RW, A new constitutive framework for arterial wall mechanics and a comparative study of material models, J. Elastic. Phys. Sci. Solid. 61 (1) (20 0 0) 1–48.

[20]. Gao H, Li WG, Cai L, Berry C, Luo XY, Parameter estimation in a holzapfel–ogden law for healthy myocardium, J. Eng. Math. 95 (1) (2015) 231–248, doi: 10.1007/s10665-014-9740-3. [PubMed: 26663931]

[21]. Li DS, Mendiola EA, Avazmohammadi R, Sachse FB, Sacks MS, A high-fidelity 3d micromechanical model of ventricular myocardium, in: International Conference on Functional Imaging and Modeling of the Heart, Springer, 2021, pp. 168–177.

[22]. Babaei H, Mendiola E, Neelakantan S, Xiang Q, Vang A, Dixon R, Shah D, Vanderslice P, Choudhary G, Avazmohammadi R, A machine learning model to estimate myocardial stiffness from edpvr, Sci. Rep. 12 (2022).

[23]. Mendiola EA, Wang E, Leatherman A, Xiang Q, Neelakantan S, Vanderslice P, Avazmohammadi R, A micro-anatomical model of the infarcted left ventricle border zone to study the influence of collagen undulation, in: Functional Imaging and Modeling of the Heart, Springer Nature Switzerland, Cham, 2023, pp. 34–43.

[24]. Avazmohammadi R, Hill MR, Simon MA, Zhang W, Sacks MS, A novel constitutive model for passive right ventricular myocardium: evidence for myofiber–collagen fiber mechanical coupling, Biomech. Model. Mechanobiol. 16 (2) (2017) 561–581. [PubMed: 27696332]

[25]. Klotz S, Hay I, Dickstein ML, Yi G-H, Wang J, Maurer MS, Kass DA, Burkhoff D, Single-beat estimation of end-diastolic pressure-volume relationship: a novel method with potential for noninvasive application, Am. J. Physiol.-Heart Circulat. Physiol. 291 (1) (2006) H403–H412.

[26]. Althouse A, Below J, Claggett B, Cox N, de Lemos J, Deo R, Duval S, Hachamovitch R, Kaul S, Keith S, Secemsky E, Teixeira-Pinto A, Roger V, Recommendations for statistical reporting in cardiovascular medicine: a special report from the american heart association, Circulation 144 (4) (2021) e70–e91, doi: 10.1161/CIRCULATIONAHA.121.055393. [PubMed: 34032474]

[27]. Torres W, Barlow S, Moore A, Freeburg L, Hoenes A, Doviak H, Zile M, Shazly T, Spinale F, Changes in myocardial microstructure and mechanics with progressive left ventricular pressure overload, JACC: Basic Transl. Sci. 5 (5) (2020) 463–480, doi: 10.1016/j.jacbts.2020.02.007. [PubMed: 32478208]

[28]. Avazmohammadi R, Hill M, Simon M, Sacks M, Transmural remodeling of right ventricular myocardium in response to pulmonary arterial hypertension, APL Bioeng. 1 (1) (2017) 016105, doi: 10.1063/1.5011639. [PubMed: 30417163]

[29]. Glower D, Spratt J, Snow ND, Kabas JS, Olsen CO, Tyson GS, Sabiston DC Jr, Rankin JS, Linearity of the frank-starling relationship in the intact heart: the concept of preload recruitable stroke work, Circulation 71 (5) (1985) 994–1009. [PubMed: 3986986]

[30]. Hanna A, Shinde A, Li R, Alex L, Humeres C, Balasubramanian P, Frangogiannis N, Collagen denaturation in the infarcted myocardium involves temporally distinct effects of mt1-mmp-dependent proteolysis and mechanical tension, Matrix Biol. 99 (2021) 18–42, doi: 10.1016/j.matbio.2021.05.005. [PubMed: 34048934]

[31]. Holmes J, Nuñez J, Covell J, Functional implications of myocardial scar structure, Am. J. Physiol. Heart Circ. Physiol. 272 (1997). H2123–30

[32]. Costa K, Holmes J, Mcculloch A, Modelling cardiac mechanical properties in three dimensions, Philos. Trans. R. Soc. Lond. Ser. A: Math. Phys. Eng. Sci. 359 (2001) 1233–1250, doi: 10.1098/rsta.2001.0828.

[33]. Omens J, Miller T, Covell J, Relationship between passive tissue strain and collagen uncoiling during healing of infarcted myocardium, Cardiovasc. Res. 33 (2) (1997) 351–358, doi: 10.1016/S0008-6363(96)00206-4. [PubMed: 9074699]

[34]. Neelakantan S, Kumar M, Mendiola EA, Phelan H, Serpooshan V, Sadayappan S, Avazmohammadi R, Multiscale characterization of left ventricle active behavior in the mouse, Acta Biomaterialia 162 (2023) 240–253. [PubMed: 36963596]

[35]. Rumberger J, Ventricular dilatation and remodeling after myocardial infarction, Mayo Clinic Proc. 69 (7) (1994) 664–674, doi: 10.1016/S0025-6196(12)61345-7.

[36]. Grossman W, Jones D, McLaurin L, Wall stress and patterns of hypertrophy in the human left ventricle, J. Clin. Investigat 56 (1) (1975) 56–64, doi: 10.1172/JCI108079.

[37]. Torres W, Jacobs J, Doviak H, Barlow S, Zile M, Shazly T, Spinale F, Regional and temporal changes in left ventricular strain and stiffness in a porcine model of myocardial infarction, Am. J. Physiol.-Heart Circulat. Physiol. 315 (4) (2018) H958–H967.

[38]. Mangion K, Carrick D, Carberry J, Mahrous A, McComb C, Oldroyd K, Eteiba H, Lindsay M, McEntegart M, Hood S, Petrie M, Watkins S, Davie A, Zhong X, Epstein F, Haig C, Berry C, Circumferential strain predicts major adverse cardiovascular events following an acute ST-segmentelevation myocardial infarction, Radiology 290 (2) (2019) 329–337, doi: 10.1148/radiol.2018181253. [PubMed: 30457480]

[39]. Espe E, Aronsen J, Eriksen M, Sejersted O, Zhang L, Sjaastad I, Regional dysfunction after myocardial infarction in rats, Circulation: Cardiovasc. Imag. 10 (9) (2017) e005997, doi: 10.1161/CIRCIMAGING.116.005997.

[40]. Chen J, Ceholski D, Liang L, Fish K, Hajjar R, Variability in coronary artery anatomy affects consistency of cardiac damage after myocardial infarction in mice, Am. J. Physiol.-Heart Circulat. Physiol. 313 (2) (2017) H275–H282, doi: 10.1152/ajpheart.00127.2017.

[41]. Sun Y, Kiani M, Postlethwaite A, Weber K, Infarct scar as living tissue, Basic Res. Cardiol. 97 (2002) 343–347. [PubMed: 12200633]

[42]. Yu J, Gu Y, Du K, Mihardja S, Sievers R, Lee R, The effect of injected rgd modified alginate on angiogenesis and left ventricular function in a chronic rat infarct model, Biomaterials 30 (5) (2009) 751–756, doi: 10.1016/j.biomaterials.2008.09.059. [PubMed: 19010528]

[43]. Dorsey S, McGarvey J, Wang H, Nikou A, Arama L, Koomalsingh K, Kondo N, Gorman J, Pilla J, Gorman R, Wenk J, Burdick J, Mri evaluation of injectable hyaluronic acid-based hydrogel therapy to limit ventricular remodeling after myocardial infarction, Biomaterials 69 (2015) 65–75, doi: 10.1016/j.biomaterials.2015.08.011. [PubMed: 26280951]

[44]. Zhu Y, Wood N, Fok K, Yoshizumi T, Park D, Jiang H, Schwartzman D, Zenati M, Uchibori T, Wagner W, Riviere C, Design of a coupled thermoresponsive hydrogel and robotic system for postinfarct biomaterial injection therapy, Annal. Thoracic Surg. 102 (3) (2016) 780–786, doi: 10.1016/j.athoracsur.2016.02.082.

[45]. Li D, Avazmohammadi R, Rodell C, Hsu E, Burdick J, Gorman J, Gorman R, Sacks M, How hydrogel inclusions modulate the local mechanical response in early and fully formed post-infarcted myocardium, Acta Biomaterialia 114 (2020) 296–306, doi: 10.1016/j.actbio.2020.07.046. [PubMed: 32739434]

[46]. Ifkovits J, Tous E, Minakawa M, Morita M, Robb J, Koomalsingh K, Gorman J, Gorman R, Burdick J, Injectable hydrogel properties influence infarct expansion and extent of postinfarction left ventricular remodeling in an ovine model, Proc. Natl. Acad. Sci. 107 (25) (2010) 11507–11512, doi: 10.1073/pnas.1004097107. [PubMed: 20534527]

[47]. Chung E, Dan D, Solomon S, Bank A, Pastore J, Iyer A, Berger R, Franklin J, Jones G, Machado C, Stolen C, Effect of peri-infarct pacing early after myocardial infarction, Circulation: Heart Failure 3 (6) (2010) 650–658, doi: 10.1161/CIRCHEARTFAILURE.110.945881. [PubMed: 20852059]

[48]. Bonnemain J, Del Nido P, Roche E, Direct cardiac compression devices to augment heart biomechanics and function, Annu. Rev. Biomed. Eng. 24 (2022) 137–156. [PubMed: 35395165]

[49]. Mazur W, Krzyzak A, Hennel F, Diffusion-weighted imaging and diffusion tensor imaging of the heart in vivo: major developments, Adv. Intervent. Cardiol./Postepy w Kardiologii Interwencyjnej 18 (2022) 350–359, doi: 10.5114/aic.2022.121345.

[50]. Usman M, Mendiola E, Mukherjee T, Mehdi R, Ohayon J, Alluri P, Sadayappan S, Choudhary G, Avazmohammadi R, On the possibility of estimating myocardial fiber architecture from cardiac strains, in: Bernard O, Clarysse P, Duchateau N, Ohayon J, Viallon M (Eds.), Functional Imaging and Modeling of the Heart, Springer Nature Switzerland, Cham, 2023, pp. 74–83.

[51]. Hung C, Verma A, Uno H, Shin S, Bourgoun M, Hassanein A, McMurray J, Velazquez E, Kober L, Pfeffer M, Solomon S, Longitudinal and circumferential strain rate, left ventricular remodeling, and prognosis after myocardial infarction, J. Am. College Cardiol. 56 (22) (2010) 1812–1822, doi: 10.1016/j.jacc.2010.06.044.

[52]. Reindl M, Tiller C, Holzknecht M, Lechner I, Beck A, Plappert D, Gorzala M, Pamminger M, Mayr A, Klug G, Bauer A, Metzler B, Reinstadler S, Prognostic implications of global longitudinal strain by feature-tracking cardiac magnetic resonance in ST-elevation myocardial infarction, Circulation: Cardiovasc. Imag. 12 (11) (2019) e009404, doi: 10.1161/CIRCIMAGING.119.009404.

[53]. Bujak M, Kweon H, Chatila K, Li N, Taffet G, Frangogiannis N, Aging-related defects are associated with adverse cardiac remodeling in a mouse model of reperfused myocardial infarction, J. Am. Coll. Cardiol. 51 (2008) 1384–1392, doi: 10.1016/j.jacc.2008.01.011. [PubMed: 18387441]

## Statement of significance

Biomechanical and architectural adaptation of the LVFW remains a central, yet overlooked, remodeling process post-MI. Our study indicates the biomechanical adaptation of the LVFW post-MI is highly individual and driven by altered fiber network architecture and collective changes in collagen fiber content, undulation, and stiffness. Our findings demonstrate the possibility of using cardiac strains to infer such fiber-level remodeling events through in-silico modeling, paving the way for in-vivo characterization of multiscale biomechanical indices in humans. Such indices will complement the traditional, organ-level measures of LV anatomy and function that often fall short of early prognostication of heart failure in MI.

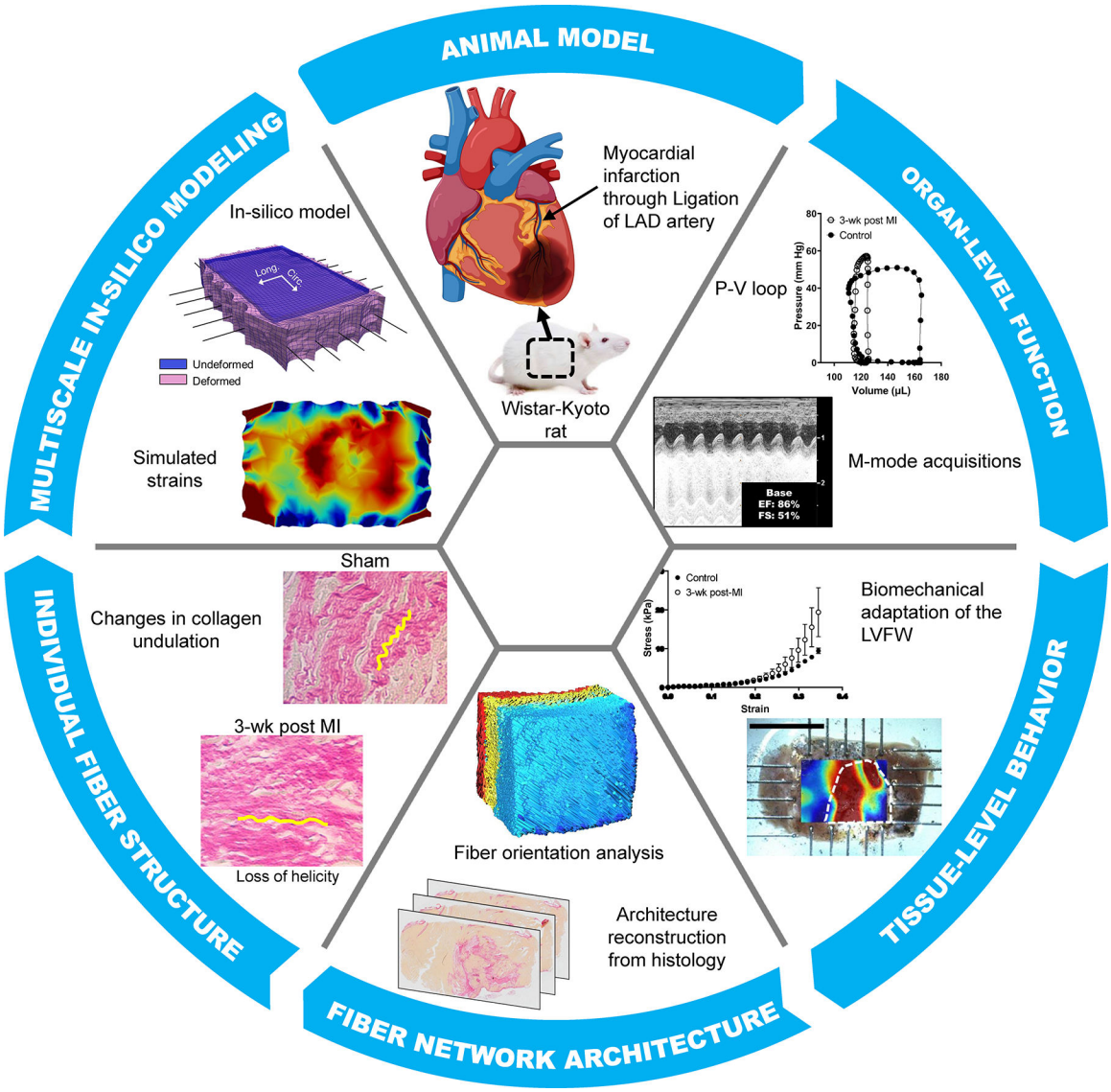


**Fig. 1.**

Left ventricular (LV) remodeling characterization methods at multiple length scales ranging from organ-level function measurements to quantifying fiber-level structural remodeling. Data from multiple length scales were assimilated to develop an in-silico predictive model to study the effects of fiber-level remodeling after MI (myocardial infarction) on LV free wall (LVFW) function. LAD: left anterior descending artery; P-V: pressure-volume.

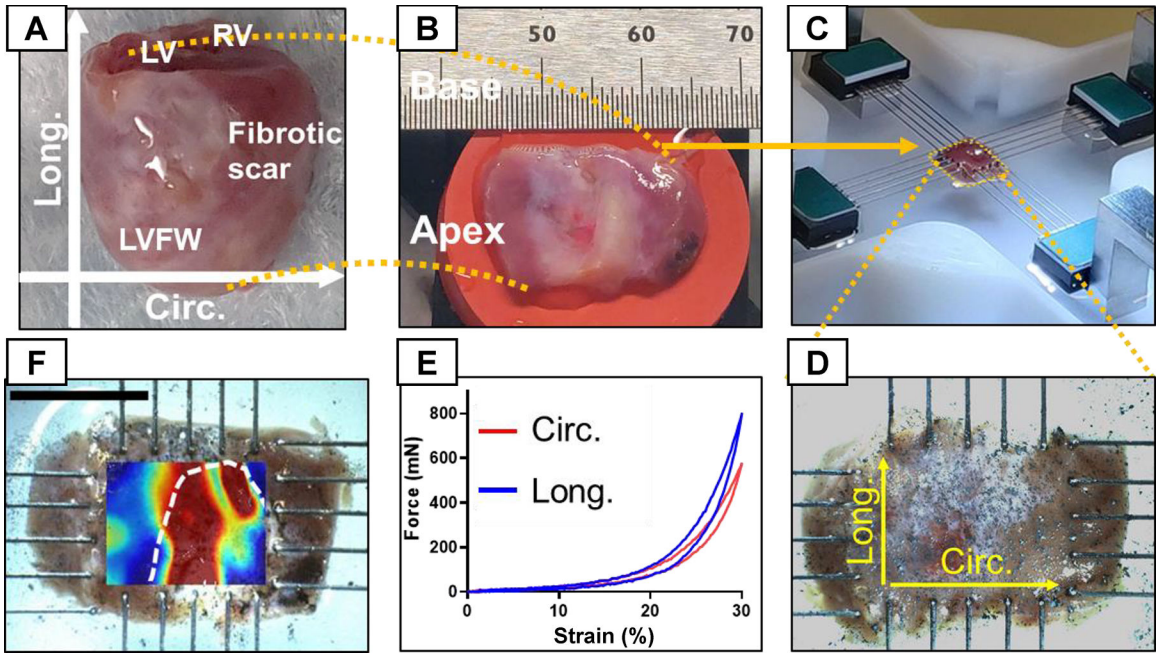


**Fig. 2.**

LVFW dissection and testing process. **(A)** Heart specimen with the atria removed. **(B)** Excised LVFW with apex and base labeled. **(C)** Mechanical testing of the LVFW specimens subjected to biaxial tensile loads using 5-rake tines per side. **(D)** Magnified image of LVFW testing with directions marked for reference. A dense, random, and multi-sized spread of graphite powder was used to obtain the regional strain field in LVFW specimens using DIC. **(E)** Representative force-strain relationship obtained from biaxial testing. **(F)** Representative strain contour obtained from DIC imaging of a 3-wk specimen. The white dashed line approximates the scar region identified from histology. Circ: circumferential direction; Long: longitudinal direction; LV: left ventricle; LVFW: left ventricle free-wall; RV: right ventricle; DIC: digital image correlation.

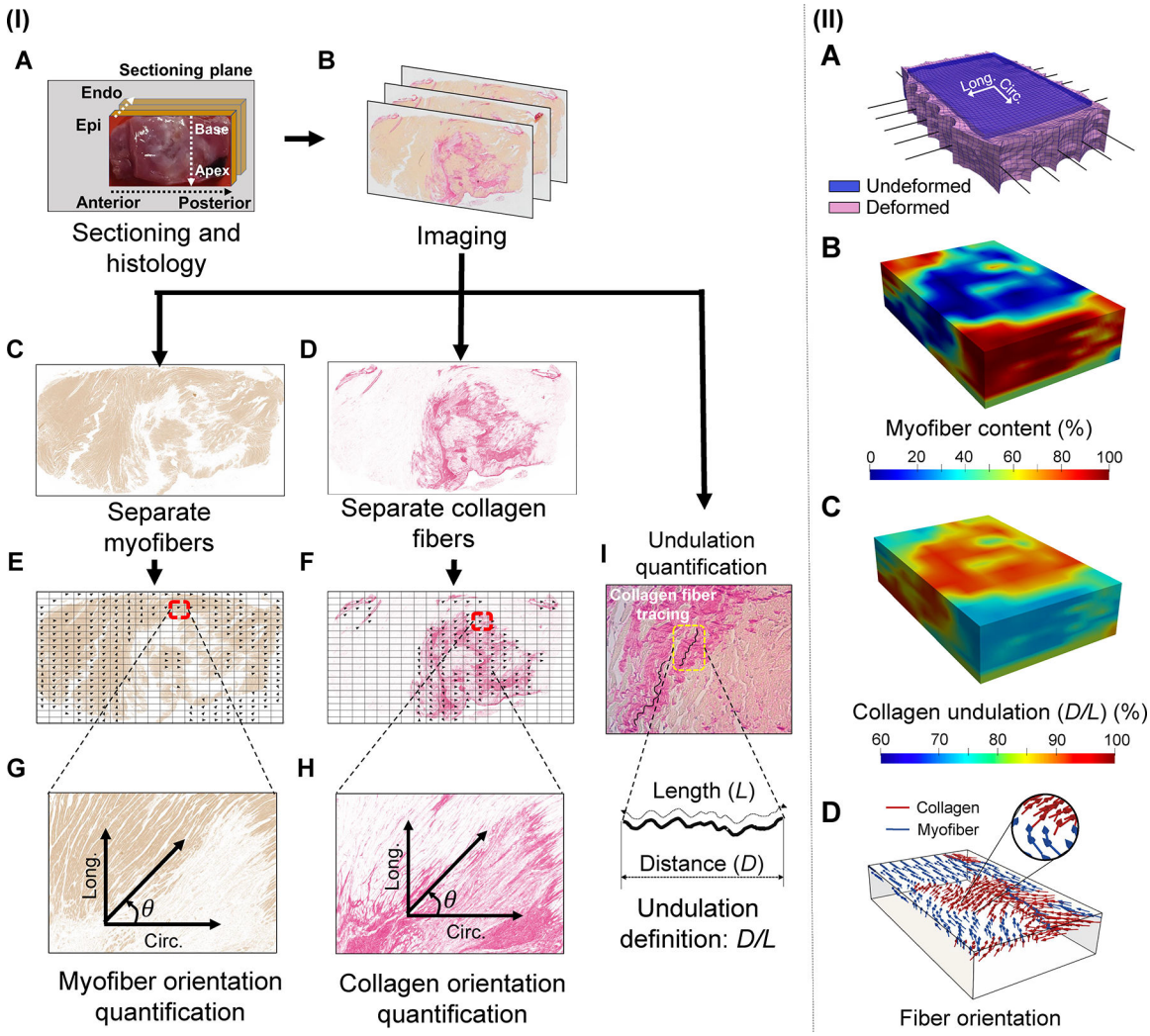


**Fig. 3.**

(**I**) Methods used to quantify fiber-level remodeling events. LVFW tissues were sectioned transmurally and stained using picrosirius red (PSR). The myofiber and collagen fiber parts of the image were separated and analyzed to obtain fiber orientation distribution. Histological slides were also imaged at a higher magnification, 40x, to quantify the amount of slack observed in collagen fibers. Representative images belong to a 3-wk post-MI specimen. (**II**) (A) Rat-specific in-silico LVFW model geometry at the initial (blue) and final deformed state (pink) once displacements were applied to the simulated rakes (black line elements). (B) Representative visualization of the 3-D spatial myofiber content and (C) collagen undulation data incorporated into the in-silico model. (D) Representative visualization indicating the regional myofiber (blue) and collagen fiber (red) architecture derived from histology and incorporated in the LVFW slab model. Visualizations presented correspond to a 2-wk post-MI specimen.

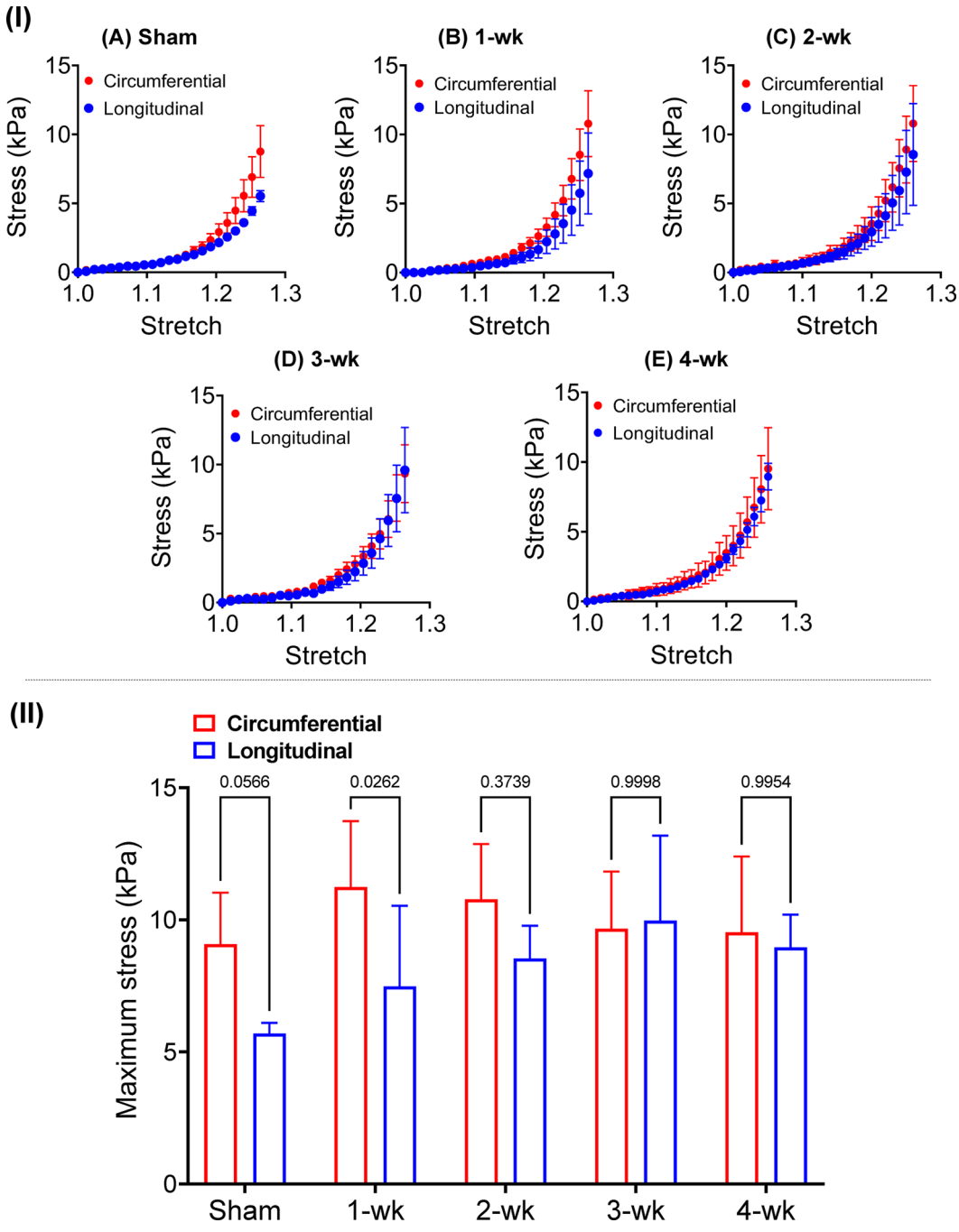


**Fig. 4.**

**(I)** Stress-stretch plots obtained from biaxial testing of LVFW specimens excised after **(A)** sham surgery, **(B)** 1-wk post-MI, **(C)** 2-wk post-MI, **(D)** 3-wk post-MI, and **(E)** 4-wk post-MI. **(II)** Maximum stress in the circumferential and longitudinal directions indicated reduced anisotropy in later time-points. Statistical significance was performed by two-way ANOVA with Šidák's correction for multiple comparisons. (n = 6 at each time-point).

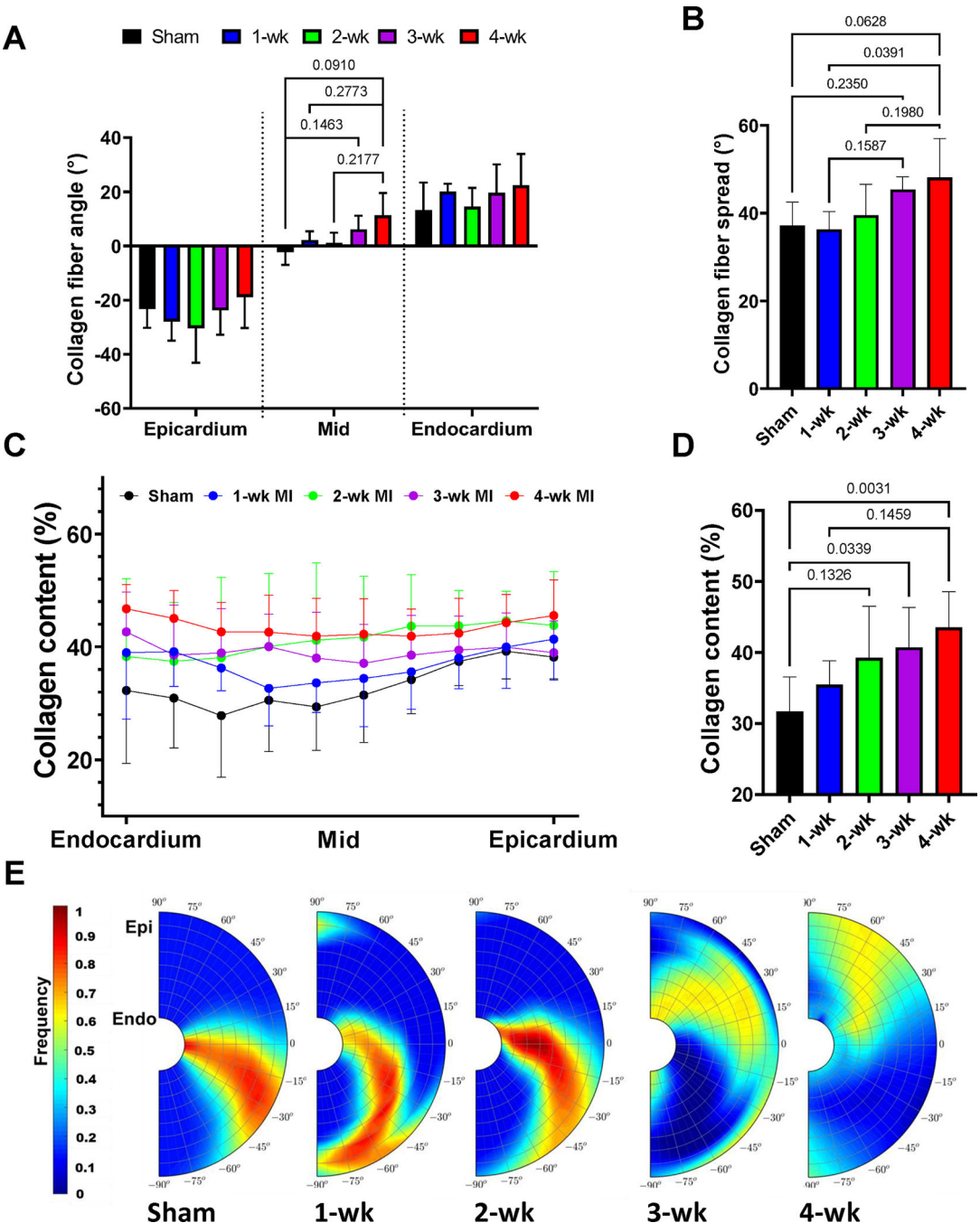


**Fig. 5.**

**(A)** Mean collagen fiber angle at several transmural depths. **(B)** Mean collagen fiber spread of the entire LVFW at various post-MI time-points. **(C)** Transmural collagen content at sham and post-MI time-points. **(D)** Mean collagen volume fraction of the entire LV free wall at various post-MI time-points. **(E)** Representative collagen fiber orientation plots for each time-point. Statistical significance was calculated by performing ordinary one-way ANOVA with Tukeys multiple comparison test. (n = 6 at each time-point).

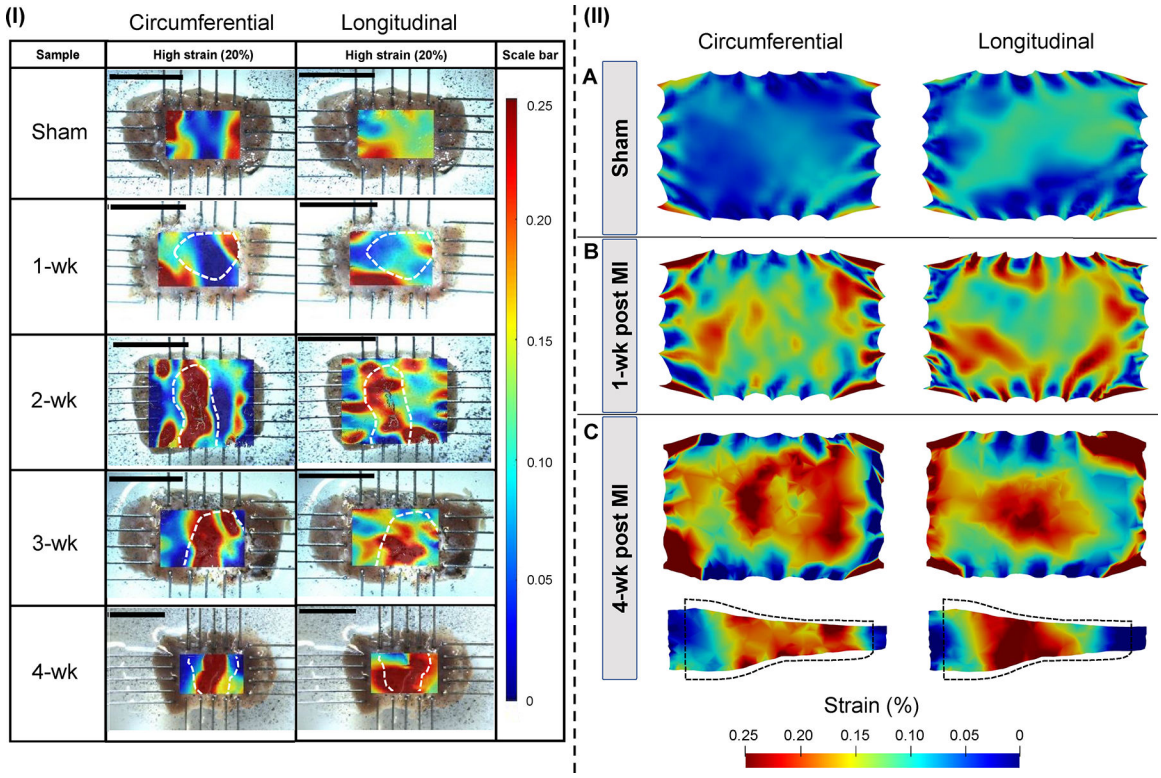


**Fig. 6.**

(**I**) Circumferential and longitudinal strain measurements calculated by digital image correlation (DIC). Strains are reported at 20% equibiaxial strain. Infarct scar regions identified through histology are marked in white dashed lines. Scale bars indicate 10 mm. (**II**) Simulated circumferential and longitudinal strain distributions visualized at the (A) sham, (B) 1-wk, and (C) 4-wk time-points for models with subject-specific regional thickness. Regional strains are reported at 20% loading strain and visualized at a central 2-D cross-section. Side-view 2-D cross-sections are also presented for 1-wk and 4-wk results; the black dashed line indicated the undeformed state.

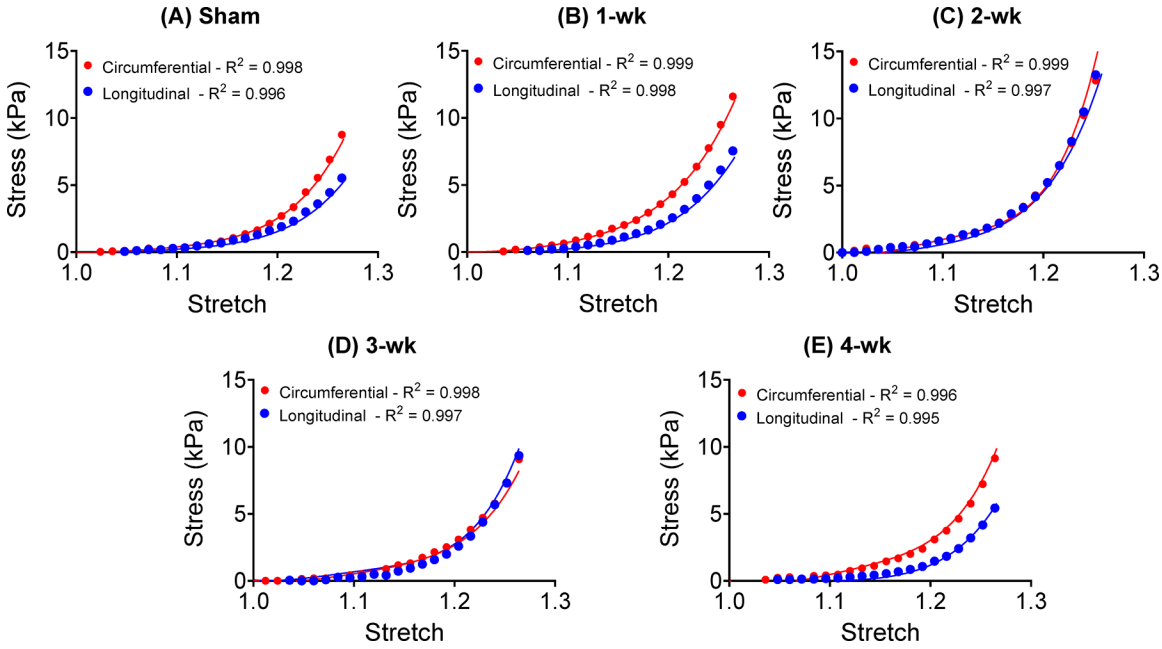


**Fig. 7.**

Subject-specific biaxial test data (markers) and fitted stress-stretch response (lines) generated by *in-silico* models incorporating fiber content and orientation distribution obtained from histology.

**Table 1**

Mean and standard deviation of the strain magnitude at the end of the toe region of the biaxial response calculated as the strain at which tissue stress was equal to 10% maximum stress. No statistically significant differences were found between time- points. Green strain is related to the stretch via $\lambda = \sqrt{2E + 1}$

| | Maximum Toe-Region Strain (%) |
|---|---|
| Sham | 12.5 ± 1.08 |
| 1-wk | 14.8 ± 2.95 |
| 2-wk | 13.8 ± 3.74 |
| 3-wk | 12.9 ± 2.10 |
| 4-wk | 12.7 ± 6.10 |

**Table 2**

Measured thickness of LVFW specimens at remote and infarct regions. Data is presented as mean ± standard deviation. One-way ANOVA with Dunnett's multiple comparison test was conducted with the thickness ratio data; mean infarct- to-remote thickness ratios were compared with a control value of 1.

| | Remote Thickness (mm) | Infarct Thickness (mm) | Thickness Ratio |
|---|---|---|---|
| Sham | 3.14 ± 1.03 | - | - |
| 1-wk | 2.34 ± 1.42 | 1.93 ± 1.25 | 0.82 ± 0.07 * |
| 2-wk | 3.58 ± 0.37 | 3.18 ± 0.28 | 0.89 ± 0.05 |
| 3-wk | 3.23 ± 1.35 | 1.75 ± 0.83 | 0.53 ± 0.11 **** |
| 4-wk | 2.40 ± 0.87 | 1.69 ± 0.89 | 0.59 ± 0.19 **** |

* $p < 0.025$,

**** $p < 0.0001$.

**Table 3**

Passive material parameters estimated by the finite-element tissue models using subject-specific regional thickness at each time-point. Parameters $\lambda_s$ and $\Phi_C$ characterize the mean collage slack stretch and volume fraction, respectively, and were calculated from imaging and used as inputs. The ratio denotes the infarct-to-remote thickness ratio.

| | $a_m$ (*kPa*) | $b_m$ | $a_c$ (*kPa*) | $b_c$ | $\lambda_s$ | $\Phi_C$ | Thickness Ratio |
|---|---|---|---|---|---|---|---|
| Sham | 3.36 | 0.96 | 17.9 | 3.58 | 1.184 | 0.14 | - |
| 1-wk | 6.21 | 0.11 | 5.53 | 0.28 | 1.068 | 0.15 | 0.85 |
| 2-wk | 2.92 | 0.06 | 6.65 | 0.04 | 1.055 | 0.60 | 0.70 |
| 3-wk | 1.97 | 0.04 | 1.38 | 1.56 | 1.095 | 0.21 | 0.45 |
| 4-wk | 1.52 | 0.013 | 1.10 | 0.018 | 1.043 | 0.16 | 0.52 |